RSC Advances




ROYAL SOCIETY OF CHEMISTRY

www.rsc.org/advances

Journal Name

ARTICLE

# Use of Morphological Features of Carbonaceous Materials for Improved Mechanical Properties of Epoxy Nanocomposites

Received 00th January 20xx,
Accepted 00th January 20xx

DOI: 10.1039/x0xx00000x

www.rsc.org/

R. Atif, J. Wei, I. Shyha, F. Inam*

The objective of this work was to study the influence of reinforcement morphology on damage tolerance and fracture toughness of epoxy based nanocomposites. Two different forms of carbonaceous reinforcements were used: multi-layered graphene (MLG) and nanostructured graphite (NSG). The maximum increase in Young's modulus was observed from 609.6 MPa to 766 MPa (25.7% increase) in case of 0.1 wt% NSG. The NSG showed maximum increase in hardness up to 7.9% while MLG showed up to 18.3%. The MLG and NSG increased the storage modulus and $T_g$ while loss modulus and Tanδ decreased with MLG and NSG. SEM images of fractured surfaces of tensile specimens showed that fracture mode was significantly altered by MLG and NSG.

## Introduction

The exploitation of morphologically modified geometries in synthetic and bioinspired materials is a novel area of research.[1–3] The morphologically modified carbonaceous materials are produced by various methods and have found numerous applications.[4–6] It was shown that the superior electronic properties of graphene are sensitive to surface features.[7] Through their crack deflection modeling, Faber and Evans showed that maximum improvement in fracture toughness, among all other nano-reinforcements, can be obtained using graphene mainly because of its better capability of deflecting the propagating cracks.[8,9] The graphene sheets have coiled structure that helps them to store sufficient amount of energy.[10,11] The individual sheet and chunk of sheets together are subjected to plastic deformation at the application of external load. The applied energy is utilized in undertaking plastic work that enhances the material's ability to absorb more energy.[12] Graphene has shown inclination for stable folding and bending energy at folds is compensated by intersheet adhesion (Van der Waals interactions).[13] The individual layers of graphene, under external loadings and thermal stresses, undergo out-of-plane wrapping,[14] rippling,[15] folding,[16] scrolling,[17] and crumpling,[18] making graphene suitable to enhance the toughness of polymers. These phenomena can be observed experimentally and explored using computer simulations.[19,20] Although various methods have been employed to produce morphologically modified carbonaceous materials and explored for various applications, an obvious gap in the literature can clearly be observed regarding detailed study about influence of morphology on damage tolerance and fracture toughness of polymers. The damage tolerance is the ability of a critical structure to withstand a level of service or manufacturing-induced damage or flaws while maintaining its function.[21] The ability of a material containing crack to resist fracture, known as fracture toughness, is a simple yet trustworthy indicator of the material's damage tolerance and hindrance against fracture, and is considered as one of the most important mechanical properties.

In this work, two different forms of carbonaceous materials were explored: multi-layered graphene (MLG) and nanostructured graphite (NSG). The NSG had wide particle size distribution compared with MLG. Multi-layered graphene-epoxy (MLG-EP) and nanostructured graphite-epoxy (NSG-EP) samples were produced. The measured properties indicate that the performance of produced nanocomposites is strongly dependent on the morphological features of nanocomposites.

## Experimental Section

### Materials

NSG of thickness 10-300 nm and lateral size 100-500 nm with specific surface area of 250 $m^2g^{-1}$ and purity 99% was purchased from Graphene Supermarket. MLG of 12 nm average thickness and 4.5 µm average lateral size with specific surface area of 80 $m^2g^{-1}$ and purity 99.2% was purchased from Graphene Supermarket. Both filler were washed extensively with acetone to remove any impurities and tip sonicated for 6 h to fragment any aggregates. Bisphenol A-epichlorohydrin based epoxy having density of ~1.3 $gcm^{-3}$ resin was purchased from Polyfibre suppliers. Dimethylbenzylamine isophorone diamine based low viscosity fast curing hardener with ~1.1 $gcm^{-3}$ density was used to cure the epoxy and purchased from Polyfibre suppliers. The low viscosity of the

*Department of Mechanical and Construction Engineering, Faculty of Engineering and Environment, City Campus, Northumbria University, Newcastle upon Tyne, NE1 8ST, United Kingdom. Email: fawad.inam@northumbria.ac.uk*

Electronic Supplementary Information (ESI) available: [details of any supplementary information available should be included here]. See DOI: 10.1039/x0xx00000x

hardener helped improving the dispersion state and the fast curing helped prevention of reinforcement agglomeration. The gelation time of the resin was 43 min at room temperature (RT).

### Samples production

The MLG and NSG of different weight fractions (0.1 wt%, 0.3 wt%, 0.5 wt%, and 1.0 wt%) were taken and dispersed in hardener at RT using tip sonication for 3 h. The reinforcement dispersed hardener and epoxy were vacuum degassed separately for 30 min. Then, the resins were mixed in epoxy: hardener ratio of 2:1. Following thorough hand mixing for 10 min, vacuum degassing was again carried out for 15 min. The resin was poured into molds and cured at room temperature for 6 h followed by post-curing at 80 °C for 6 h.

### Characterization

The densification of samples was calculated according to ASTM Standard D792. The densities of epoxy, hardener, MLG, NSG, and water were, 1.3, 1.1, 2.26, 2.26, and 0.9975 gcm$^{-3}$, respectively. Vickers microhardness test was conducted using Buehler Micromet II to determine the hardness values of samples. A load of 200 g was applied for 10 seconds. Light transmittance in the UV-Visible spectroscopy (HITACHI U-3000) was used to quantify the dispersion state of MLG at fixed wavelength of 450 nm. Standard polystyrene cuvettes with an optical path length of 10 mm were used for transmittance measurement. To determine the influence of sonication on particle size and possible delayering, particle size of MLG and NSG before and after sonication was measured using Malvern Mastersizer 2000. The sonication was carried out using tip sonicator of power 750 W and frequency 250 kHz (Vibra-cell model VC 750, USA). The operation mode was 70% power with 10 s vibration and 5 s break.

Tensile, three point bend, and fracture toughness tests were conducted using Instron Universal Testing Machine (Model 3382). The displacement rate was kept 1 mmmin$^{-1}$ for all three tests. Five specimens were tested for each composition. Tensile properties were measured according to ASTM D638 Type-V geometry with specimen thickness 4 mm. Three point bend test was conducted according to ASTM D790 with specimen dimensions 3 × 12.7 × 48 mm. A single-edge-notch three point bending (SEN-TPB) specimen was used to determine mode-I fracture toughness ($K_{1C}$) according to ASTM D5045. The specimen dimensions were 3 × 6 × 36 mm with a crack of length 3 mm. The notch was made at the mid of sample and tapped to sharpen by a fresh razor blade. The $K_{1C}$ was calculated using Equation (1),

$$K_{1C} = \frac{P_{max} f\left(\frac{a}{w}\right)}{BW^{1/2}} \quad (1)$$

where, $P_{max}$ is maximum load of load-displacement curve (N), f(a/w) is constant related to geometry of the sample and was calculated using Equation (2), B is sample thickness (mm), W is sample width (mm), and a is crack length (kept between 0.45W and 0.55W). The critical strain energy release rate ($G_{1C}$) was calculated using Equation (3) where E is the Young's modulus obtained from the tensile tests (MPa), and v is the Poisson's ratio of the polymer, taken to be 0.35.

$$f(a/w) = \frac{\left[\left(2+\frac{a}{w}\right)\left\{0.0866+4.64\left(\frac{a}{w}\right)-13.32\left(\frac{a}{w}\right)^2+14.72\left(\frac{a}{w}\right)^3-5.6\left(\frac{a}{w}\right)^4\right\}\right]}{\left(1-\frac{a}{w}\right)^{3/2}} \quad (2)$$

$$G_{1C} = \frac{K_{1C}^2(1-\nu^2)}{E} \quad (3)$$

Charpy impact toughness test was carried out according to ASTM D6110 using notched specimen with dimensions 3.2 × 12.7 × 64 mm. A V-notch (45°) was made in the middle of the specimen whose depth was 2.5 mm and tip radius of 0.25 mm. The specimen was placed as simply supported beam and hit by hammer from behind the notch. The impact toughness was calculated using Equation (4),

$$Impact\ toughness = \frac{mgh(\cos\beta-\cos\alpha)}{wt} \quad (4)$$

where, m is hammer mass (kg), g is standard gravity (9.8 ms$^{-2}$), h is length of hammer arm (m), β is hammer swing up angle after test piece broken (rad), α is hammer lifting up angle (rad), w is sample width (mm), and t is sample thickness (mm). DMA (Model 8000, PerkinElmer) was used to determine dynamic storage modulus (É), and loss modulus (E") of the samples. The loss factor Tanδ was calculated as the ratio (E"/ É). Rectangular test specimens of dimensions 2.5 × 8 × 30 mm were used with a single cantilever clamp. All tests were carried out by temperature sweep method (temperature ramp from 30 °C to 180 °C at 10 °Cmin$^{-1}$) at a constant frequency of 1 Hz. The glass transition temperature ($T_g$) was taken as the temperature value at the peak of Tanδ curves. Scanning electron microscopy analysis using SEM FEI Quanta 200, was carried out of the fractured surfaces of tensile specimens to evaluate the fracture modes in the samples. The fractured portions were cut from the specimens and a layer of gold was applied using Emscope sputter coater model SC500A.

## Results and Discussion

The SEM images of as-received MLG and NSG are shown in Fig. 1 (a,b,c) and (d,e,f), respectively. It can be observed that NSG is finer and has wider particle size distribution than MLG. The MLG has wrinkles on its surface while NSG has more corrugated and porous structure. The wide particle size distribution of NSG is helpful for strong interfacial bonding and mechanical interlocking. To determine the dispersion state of reinforcement in different media as a function of sonication time, reinforcement was dispersed in three different media: (a) epoxy (EP), (b) hardener (HD), and (c) mixture of epoxy and hardener (EP+HD). The sonication process was carried out up to 1 h. The MLG dispersed in epoxy and hardener is shown in Fig. 2 and light absorption trends are shown in Fig. 3 (a). The graph shows a significant increase in light absorbance for the MLG dispersed in hardener (HD) within the first 12 min. This high magnitude slope suggests a relatively higher tendency of MLG to disperse uniformly in hardener. Before sonication, MLG is present in agglomerated form which lowered the light absorbance as most of the light was able to transmit through transparent suspension media. However, the dispersion state significantly improved after sonication and a larger portion of the suspension media contained dispersed reinforcement. Because of the opacity

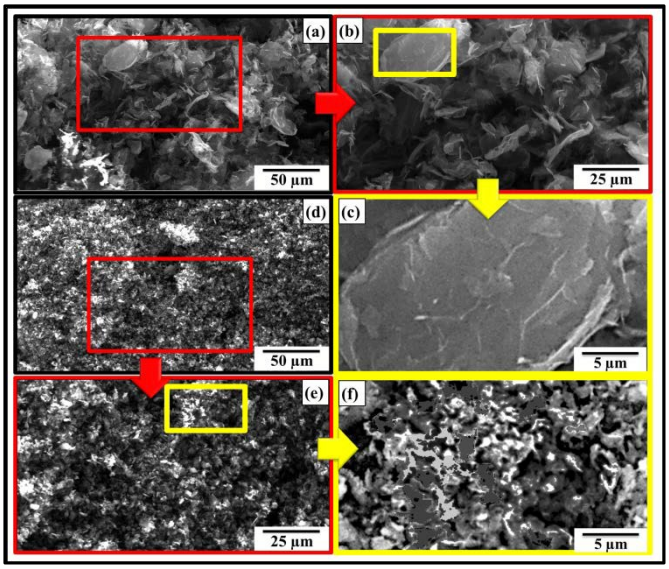


**Fig. 1** SEM images: (a,b,c) MLG, and (d,e,f) NSG.

of graphene, a little shard of light was transmitted and most of the light was absorbed.[22]

A similar trend was observed for the MLG dispersed in epoxy (EP), where light transmittance also decreased with the sonication time. However, the slope is much lower than in case of hardener which can be attributed to relatively poor dispersion of MLG in epoxy compared with that in hardener. It is noteworthy that as compared to 15% drop in epoxy and 26% drop in hardener, there is just 11% drop in the transmittance for graphene dispersion in the mixture of epoxy and hardener (EP+HD). It can be attributed to the onset of curing process. The dispersion of MLG becomes difficult in high viscosity media. Therefore, lowest light absorption values were observed in case of EP+HD.

The primary objective of light absorption studies was to optimize sonication parameters. What we observed that the dispersion state nearly became constant after 30 min of sonication time. Considering this fact, sonication process for composite samples was maintained 3 h which is significantly greater than 30 min. It was to ensure nearly uniform dispersion in the samples. In addition, it was observed that dispersion state is better in hardener than in epoxy resin. Therefore, fillers were dispersed in hardener instead of epoxy. One might suggest that we could use organic solvents, such as acetone or DMF, to obtain uniform dispersion. However, it is well-established that proper removal of organic solvent may be a problem and some remnants can adversely affect the properties. [23–27] Loos et al.[28] produced epoxy samples with varied amount of acetone (0, 7, 10, 13 wt%). They reported significant drop in Young's modulus, tensile strength and fracture strain as a result of residual acetone. The drop in mechanical properties was found directly related with the amount of acetone used.[28] The traces of organic solvents influence cure kinetics and restrict crosslinking process.[29] Hong and Wu[30] mentioned that residues of organic solvents result in lower curing exotherm, reaction rate, initial curing rate, glass transition temperature ($T_g$),

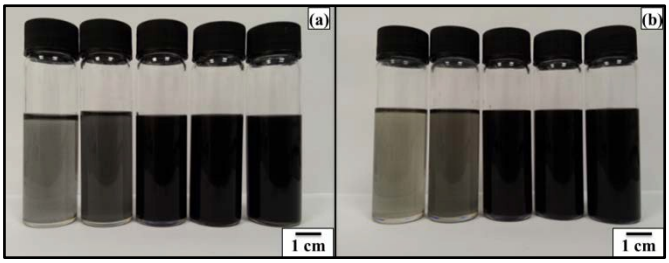


**Fig. 2** Qualitative analyses of, (a) graphene-EP and (b) graphene-HD (concentration from left to right: 0.005 wt%, 0.0125 wt%, 0.025 wt%, 0.05 wt%, 0.1 wt%).

and reaction order. They also reported that organic solvents with higher boiling points have greater effect on cure kinetics and mechanical properties of epoxy.[30]

As the title suggests, our primary objective was to study the influence of "morphological features" on mechanical properties of produced nanocomposites. Therefore, we wanted to restrict parameters as much as possible. For example, if we had used organic solvents, then questions could arise that how was it ensured that organic solvent was completely removed? If there are any remnants, then what is the porosity size in both samples as stress concentration is dependent on notch size and shape. And any change in densification is stemming from the fillers or residuum of the organic solvent? To ward these queries off, organic solvent was not used and all other parameters were meticulously fixed so that any change observed in mechanical properties could be correlated with the morphological features of the fillers.

Fig. 3 (b) shows the light absorption of MLG dispersion against storage time. The sonication was carried out for 1 h. Within the first 5 days, the behavior of MLG in EP and HD is similar. Both dispersions showed slight increment in light transmittance, which are 5% and 4% in EP and HD, respectively. This increment indicated that some level of re-aggregation took place during this time or possibly the lighter particles moved to surface of the suspension media and heavier particles settled down. Up to 10 days, the light transmittance did not change significantly indicating the dispersions remained stable during this period. The light transmittance in case of MLG dispersed in EP+HD kept constant because the system became stable after the epoxy resin was fully cured within 24 hours.

The influence of sonication on particle size of MLG and NSG is shown in Fig. 3 (c,d). The mean dimensions of MLG are 2.95 µm and that of NSG are 3.64 µm before sonication. After sonication, the mean dimensions of MLG and NSG became 0.06 µm and 0.24 µm, respectively. It can be observed that the particle size distribution of NSG is relatively wider than MLG. In addition, a significant delayering took place during sonication. During sonication, shear forces and cavitation i.e. the growth and collapse of the micrometer-sized bubbles or voids in liquids due to pressure fluctuations, act on the bulk material and induce exfoliation.[31,32] The cavitation effect during graphene dispersion requires two conditions; presence of fluids and pressure fluctuations. Once these conditions are available, it may be approximated about whether cavitation effect was observed or not from the delayering and/or reduction in mean dimensions of the filler. In current study (Fig. 3),

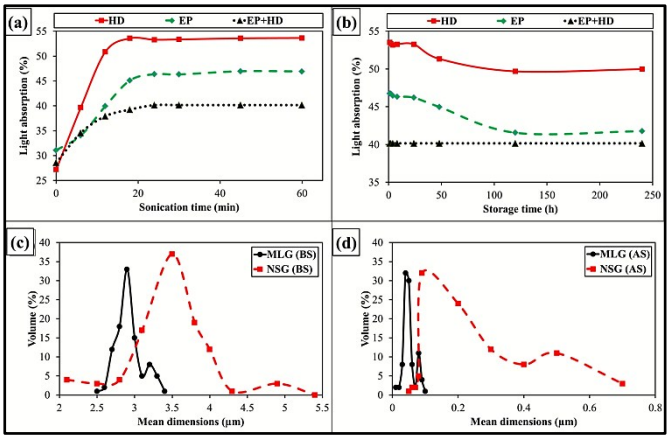


**Fig. 3** Light absorption with (a) sonication time, and (b) storage time. Mean dimensions of MLG and NSG (c) before sonication (BS), and (d) after sonication (AS).

the mean dimensions significantly reduced after sonication; therefore, it can be assumed that cavitation effect was a favorable phenomenon to occur and caused exfoliation.

The densification of samples is shown in Fig. 4 (a) where maximum densification for MLG-EP samples was observed at 0.3 wt% of MLG while at 0.1 wt% of NSG for NSG-EP samples. The decrease in densification with increase in weight fraction of MLG and NSG can be attributed to agglomeration and bridging of reinforcement particles. Voids are created inside the connected series of particles which are not filled by resin thereby causing porosity.[33] The other reason could be prevention of the escape of volatiles.[34–36]

Monolithic epoxy, because of its stiffness, cannot prevent crack propagation and is vulnerable to fracture. However, when reinforced especially by nano-fillers, such as metallic oxides,[37] clays,[38] carbon nanotubes (CNTs),[39] and other carbonaceous materials,[40] its ability to withstand crack propagation is propitiously improved and is reflected in mechanical properties of produced nanocomposites as shown in Fig. 4. The variation in Vickers microhardness is shown in Fig. 4 (b). The NSG showed maximum increase in microhardness at 0.1 wt% and microhardness increased from 287.4 Hv to 310 Hv (7.9% increase). The MLG showed maximum increase in microhardness from 287.4 Hv to 340 Hv (18.3% increase) at 0.3 wt% MLG. It shows that MLG is more effective in increasing the hardness of samples compared with NSG. The variation in Young's modulus is shown in Fig. 4 (c). The Young's modulus was increased by both MLG and NSG. The maximum increase in Young's modulus was from 609.6 MPa to 766 MPa (25.7% increase) in case of 0.1 wt% NSG. The MLG also showed significant increase in Young's modulus. The maximum increase was observed at 0.3 wt% MLG and Young's modulus increased from 609.6 MPa to 758.2 MPa (24.4% increase). The Ultimate Tensile Strength (UTS) was also significantly increased by MLG and NSG as shown in Fig. 4 (d). The maximum increase in UTS was from 45.5 MPa to 65.1 MPa (43.1% increase) in case of 0.1 wt% NSG. The MLG also showed maximum increase at 0.1 wt% and UTS increased up to 25.3%. The variation in tensile strain (%) is shown in Fig. 4 (e). The tensile strain was taken as the % value of strain corresponding to UTS. In general, the tensile strain decreases with the addition of strong and stiff reinforcement. The same trend was observed in case of MLG where tensile strain decreased with the increasing weight fraction of MLG. However, an exceptional behavior was shown by NSG where tensile strain increased with the incorporation of NSG with maximum increase observed in case of 0.1 wt% NSG. It can be attributed to mechanical interlocking. Surfaces can be made porous or rough to enhance the extent of mechanical interlocking.[41] Karger-Kocsis et al. have studied that hierarchical and hairy fillers have high surface area and capillary wetting by the polymers.[42] The textured fillers also exhibit mechanical interlocking with the polymers and cause local reinforcement of the fiber-matrix interphase.[42] Moon and Jang studied the mechanical interlocking and wetting at the interface between argon plasma treated ultra-high modulus polyethylene (UHMPE) fiber reinforced vinylester resin composite.[43] They observed a significant increase in interlaminar shear strength. It has been shown that plasma etching of UHMPE produces micro-pittings on fiber surface and this spongy surface structure helps improving the mechanical interlocking with the polymer matrix and causes a significant increase in interlaminar shear strength.[44–47] Therefore, the increase in fracture strain by NSG can be attributed to mechanical interlocking because of which the polymer chains kept elongating without fracture. The variation in flexural modulus is shown in Fig. 5 (f). The NSG showed maximum increase in flexural modulus at 0.1 wt% and flexural modulus increased from 2.33 GPa to 3.31 GPa (42.6% increase). The MLG showed maximum increase in flexural modulus at 0.3 wt% and flexural modulus increased from 2.33 GPa to 3.42 GPa (47.1% increase). The variation in flexural strength is shown in Fig. 5 (g). The maximum increase in flexural strength was observed in case of 0.1 wt% NSG where flexural strength increased from 74.3 MPa to 110.8 MPa (49.2% increase). The MLG showed maximum increase in flexural strength at 0.1 wt% and flexural strength increased from 74.3 MPa to 96.6 MPa (30.1% increase). The variation in flexural strain (%) is shown in Fig. 4 (h). The flexural strain was taken as the % value of strain corresponding to flexural strength. The flexural strain decreased with increasing weight fraction of MLG. In contrary, the NSG showed an increase in flexural strain (%). The maximum increase in flexural strain was observed at 0.3 wt% NSG and flexural strain increased from 3.4% to 4.4% (27.5% increase). The variation in mode-1 fracture toughness ($K_{1C}$) is shown in Fig. 4 (i). The maximum increase in $K_{1C}$ was from 0.85 MPa.m$^{1/2}$ to 1.2 MPa.m$^{1/2}$ (41.2% increase) in case of 0.1 wt% NSG. The MLG also showed maximum increase at 0.1 wt% and $K_{1C}$ increased from 0.85 MPa.m$^{1/2}$ to 1.1 MPa.m$^{1/2}$ (29.4% increase). The variation in critical strain energy release rate ($G_{1C}$) is shown in Fig. 4 (j). The NSG showed maximum increase at 0.1 wt% and $G_{1C}$ increased from 630.5 Jm$^{-2}$ to 685.2 Jm$^{-2}$ (8.7% increase). The MLG also showed maximum increase at 0.1 wt% and $G_{1C}$ increased from 630.5 Jm$^{-2}$ to 674.6 Jm$^{-2}$ (7% increase). The variation in Charpy impact toughness is shown in Fig. 4 (k). The NSG showed maximum increase at 0.1 wt% and Charpy impact toughness increased from 0.83 kJm$^{-2}$ to 1.503 kJm$^{-2}$ (81.1% increase). The MLG showed maximum increase at 0.3 wt% and Charpy impact toughness increased from 0.83 kJm$^{-2}$ to 1.575 kJm$^{-2}$ (89.7% increase). In most of the cases, maximum

increase in mechanical properties was observed at 0.1 wt% of the fillers. The improvement in mechanical properties is due to the reinforcing effect of carbonaceous fillers while decrease in mechanical properties can be attributed to crack generation and agglomeration. The other reason for such behavior is due to high probability of agglomeration at higher weight fractions arising from Van der Waals forces. Wang et al. have also reported that maximum improvement in mechanical properties was observed in case of 0.1 wt% of graphene oxide.[48]

The sonication time to achieve uniform dispersion may vary with increasing weight fraction of filler. In Fig. 3, it was observed that dispersion state became nearly "constant" after 30 min of sonication. However, "constant" does not mean uniform dispersion as it may be possible that applied sonication power is not enough to break all of any agglomerates present. Therefore, whether dispersion is uniform or not, cannot be quantitatively measured based on the light absorption. Therefore, literature was consulted to fix a reasonable time.[49,50] We reached the conclusion that 3 h would be enough to get a reasonable dispersion. Here, we would like to refer to title of the paper, "morphological features." As our primary objective was to correlate the mechanical properties with morphological features, therefore, sonication time would not be direct influential parameter provided that it remained the same for both the cases, which was maintained at 3 h in current work. As the mechanical properties started to decrease after 0.3 wt% of both fillers, one might suggest that 3 h sonication with other processing parameters may not be enough to achieve uniform dispersion of the fillers, especially at higher weight fractions. Future work may be carried out to study the influence of morphological features on dispersion state of varying weight fractions of fillers in different polymers.

The graphene based reinforcements affect the crosslink density of epoxy.[51] When carbonaceous materials are dispersed in polymer, the polymer chains are restricted and crosslinking is altered which

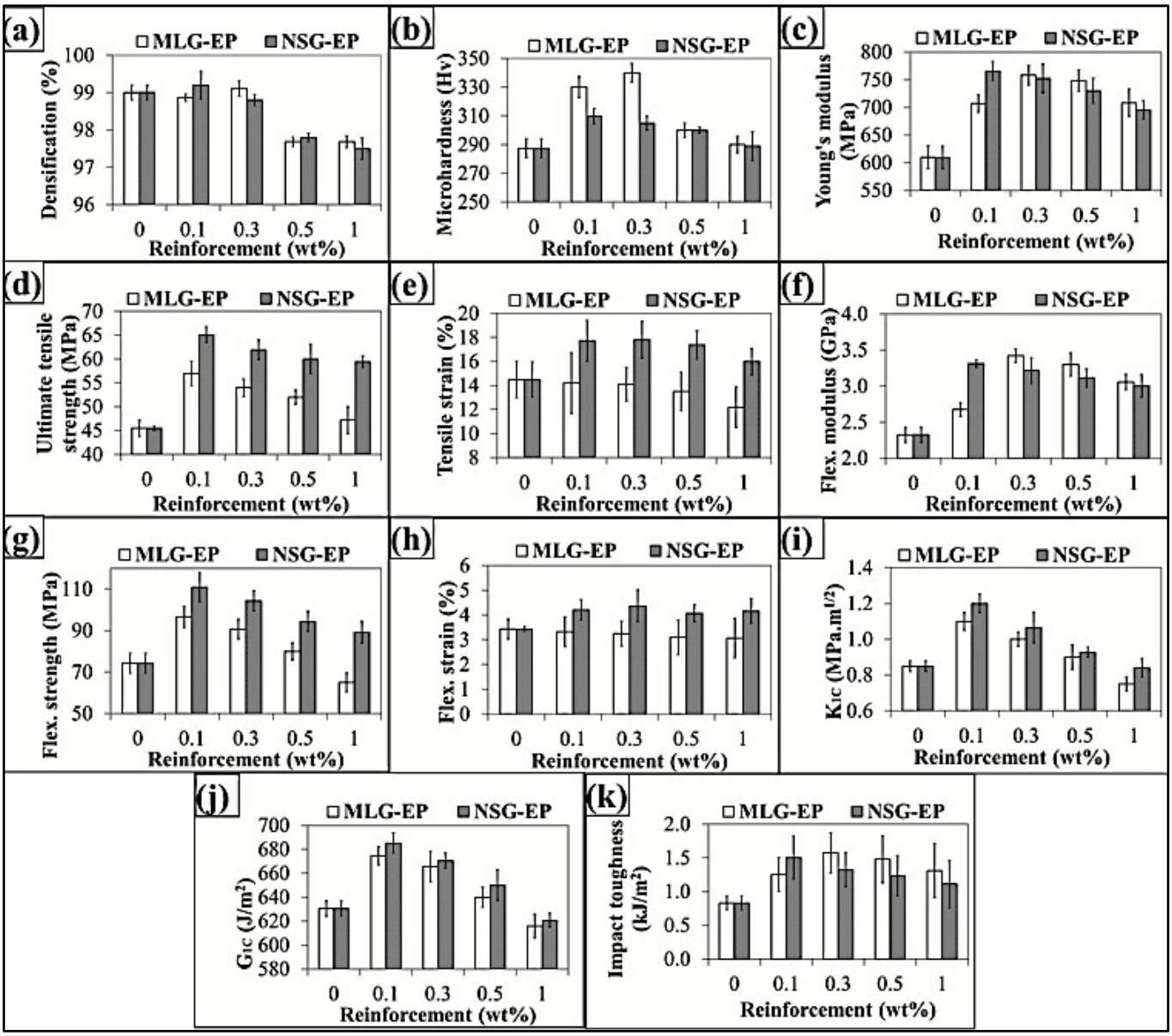


**Fig. 4** Densification and mechanical properties: (a) densification, (b) microhardness (Hv), (c) Young's modulus, (d) ultimate tensile strength, (e) tensile strain (%), (f) flexural modulus, (g) flexural strength, (h) flexural strain (%), (i) $K_{1C}$, (j) $G_{1C}$, and (k) Charpy impact toughness.

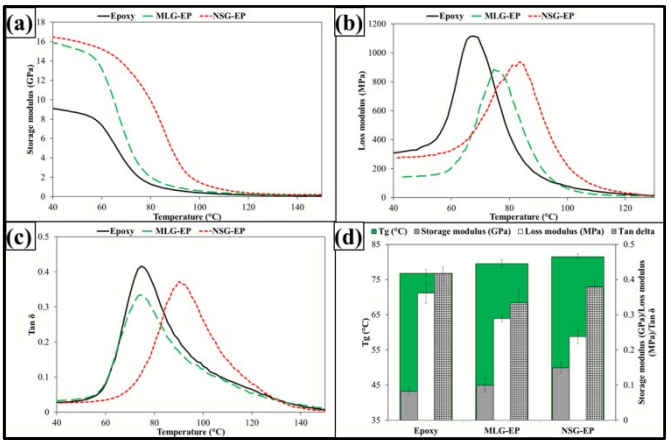


**Fig. 5** Dynamic mechanical properties: (a) storage modulus, (b) loss modulus, (c) Tanδ, and (d) $T_g$, and values of storage modulus, loss modulus and Tanδ at $T_g$.

influence the thermo-mechanical properties of nanocomposites. The influence of morphological features was also manifested in dynamic mechanical properties as shown in Fig. 5. A shift in storage modulus can be observed in Fig. 5 (a) which can be attributed to the stiffness and restriction in polymer chains caused by MLG and NSG. Because of the high stiffness of graphene, the viscous behavior of produced nanocomposites also varies as shown in Fig. 5 (b). The loss modulus was decreased by both MLG and NSG. However, a larger shift in storage and loss moduli was observed in case of NSG. The variation in Tanδ is shown in Fig. 5 (c) that shows that both MLG and NSG decreased Tanδ. One indicator of restriction in polymer chains is glass transition temperature ($T_g$) as shown in Fig. 5 (d). The $T_g$ increased from 76.5 °C to 78.5 °C in case of 0.1 wt% of MLG and up to 80.4 °C with 0.1 wt% NSG. An increase in $T_g$ with MLG and NSG shows that reinforcement is relatively uniformly dispersed. When reinforcement is uniformly dispersed, the wrinkled texture of reinforcement along with high surface area influence the maximum exothermic heat flow temperature by restricting polymer chain mobility that results in $T_g$ rise.[52] Fig. 5 (d) also shows storage modulus, loss modulus, and Tanδ values at $T_g$. It can be observed that storage modulus increased while loss modulus and Tanδ decreased with the addition of reinforcement with NSG showing more significant effect.

The DMA results are reported which give a qualitative measure of crosslink density in terms of variation in $T_g$. The $T_g$ was varied by the fillers which can be attributed to variation in crosslink density and cure kinetics due to the filler addition. However, why was the increase in $T_g$ about 2 °C in case of MLG and about 4 °C in case of NSG while filler content and processing and testing conditions were the same? This difference in $T_g$ can be attributed to morphology of the fillers as all other parameters were fixed. When we say that morphology has influence on the mechanical properties of polymers, we do not refute the fact that fillers affect the crosslink density and cure kinetics. Instead, we present the evidence that morphology of fillers is an additional factor to control the crosslink density, cure kinetics, and overall reinforcing character of fillers.

The SEM images of fractured surfaces of tensile specimens are shown in Fig. 6. Fig. 6 (a, b) show SEM images of fractured tensile

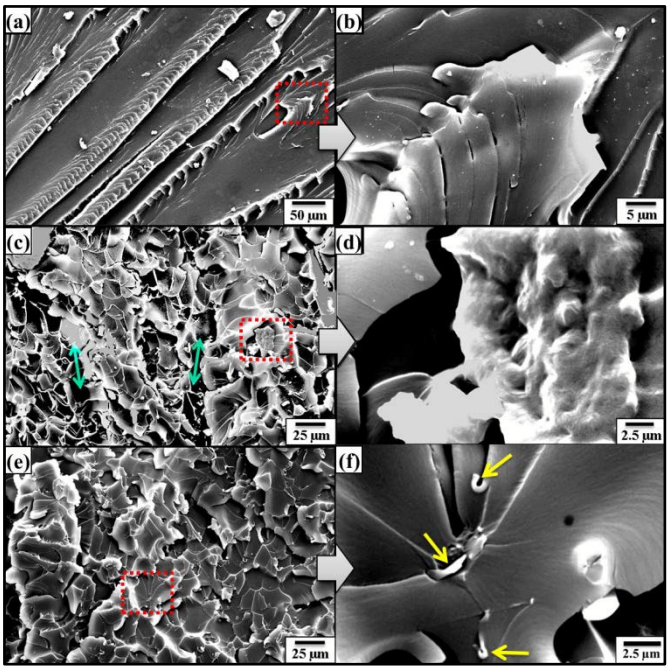


**Fig. 6** SEM images of fractured tensile specimens: (a, b) monolithic epoxy, (c, d) 0.1 wt% MLG-EP, and (e, f) 0.1 wt% NSG-EP.

specimen of monolithic epoxy. River markings can be observed which indicate that brittle fracture has taken place.[52] It is because there are no crack bridging mechanisms available in monolithic epoxy. Therefore, once crack is initiated, it propagates without any diversions and results in straight fracture paths. However, when reinforcement is introduced, fracture mode changes due to obstruction of cracks by the reinforcement. This can be observed in Fig. 6 (c,d) which show fractured tensile specimen of 0.1 wt% MLG-EP where no specific orientation of crack propagation was observed apart from a few ravines indicated by double arrows. It is because the MLG has the ability to prevent the advancement of cracks and cracks detour around the MLG to proceed.[53] The SEM images of 0.1 wt% NSG-EP tensile specimen are shown in Fig. 6 (e, f). A significant difference can be observed in fracture modes. A very rough surface can be observed with completely disparate crack orientations. It comes from the NSG reinforcement that caused the cracks to detour at each step prior to fracture. The specimen did not show straight line brittle fracture. Instead a multi-layered fracture takes place and each layer shows rough surface without any particular crack orientation. Trenches can be observed at higher magnifications with embedded NSG indicated by single arrows. This bowl-like fracture resembles dimple fracture observed in ductile metals such as aluminum. Another typical example of dimple fracture with corrugated surface is observed in low carbon steels. The low carbon steels show cup-and-cone failure which is an indication of ductile fracture.[54]

Although both MLG and NSG caused an increase in tensile and flexural properties, however, NSG showed more pronounced effect. The mechanical properties are improved when load is efficiently transferred from matrix to reinforcement. One of the controlling factors for load transfer mechanism is networking of reinforcement.

The load can only be transferred from the matrix to the reinforcement if a connected network of reinforcing particles is available. Any disjoint in the network will act as weakest link for load transfer and polymer matrix will be prone to external loading. One of the factors influencing network formation is filling ratio (or packing density). The filling ratio depends on particle size distribution and is schematically shown in Fig. 7 (a,b). When particle size distribution is narrow as shown in Fig. 7 (a), the voids between the particles would not be filled and those filler-free or empty locations will be a preferred route for the cracks to surmount the reinforcement particles. On the other hand, when reinforcement has wide size distribution as shown in Fig. 7 (b), the finer particles can occupy the empty spaces in between large particles. It increases the filling ratio and makes an efficiently connected network of reinforcement. Sohn and Moreland have shown that packing density is dependent on particle size distribution and shows a direct relationship, i.e. packing density increases as the particle size distribution is extended.[55] It was also found that packing density is independent of particle size. They also reported that particle shape also influences packing density. It is obvious as perfect cubes will have 100% packing while voids will be certain in spherical particle which will lower the packing density. Therefore, a wide size distribution is helpful in improving the mechanical properties as strong networking of reinforcing particle can take place because of high packing density. We tried hard to find solid evidence during SEM fractography analysis to come up with exact condition as schematically shown in Fig. 7 (b). We could only present a case as shown in Fig. 6 (f) where filler particles of three different sizes could be observed lying nearby but still not touching each other. The schematic condition shown in Fig. 7 (b) would be more likely in samples with very high weight fraction of filler. In current work, it

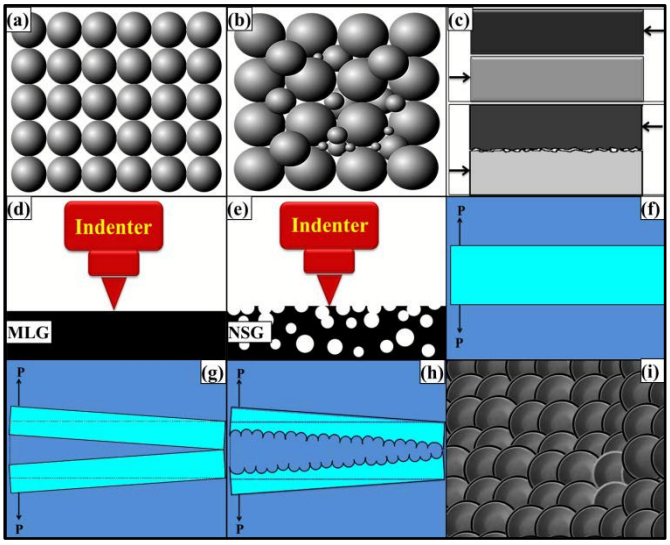


**Fig. 7** Schematics of influence of morphological features on mechanical properties and fracture modes: (a) uniform size of the particles with large voids, and (b) wide particle size distribution with efficiently connected network. (c) Smooth and rough surfaces sliding against each other. The coefficient of friction in latter case will be higher because of strong mechanical interlocking. (d) Smooth and flat MLG offers strong resistance to indenter, and (e) spongy NSG structure with relatively poor resistance against indentation (figures not drawn to scale). A comparison of brittle and dimple fracture: (f) structural member subjected to axial loading, (g) brittle fracture producing straight and smooth surfaces, (h) dimple fracture producing a corrugated surface which is an indication of ductile fracture, and (i) top view of dimple fracture.

was only 0.1 wt% which restricted the scope of observing the case where finer particles are sitting exactly in the spaces created between the larger particles. However, a slight increase in densification (Fig. 4) of NSG samples compared with MLG samples may be cited as indirect evidence that filler ratio can be increased with wide particle size distribution. The reported work of Sohn and Moreland further corroborates that filler ratio increases with extended particle size distribution.[55]

Although both MLG and NSG increased the fracture toughness, however, NSG showed higher increment. It can be attributed to the morphology and particle size distribution of NSG. By modifying the morphology, surface area of the same sized particle can be increased compared with flat and smooth particle. In addition, a porous and rough particle can significantly increase the coefficient of friction between the matrix and reinforcement. Cumberland et al. have shown that coefficient of friction depends upon morphological features of particles.[56] A large amount of energy will be dissipated to work against friction that will increase the toughness of the polymer prior to fracture. A comparison of the mechanical interlocking between smooth and rough surfaces, when subjected to shear loading, is schematically shown in Fig. 7 (c). When the reinforcement has smooth surface, the interfacial interactions will be weak that will yield inferior mechanical properties. On the contrary, when surface is rough and porous, there will be strong bonding due to mechanical interlocking and increased surface area. A large amount of energy is required to work against coefficient of friction thereby resulting in increased toughness. Therefore, controlled morphological features and wide particle size distribution are preferable with large surface area and enhanced interfacial interactions to engender superior mechanical properties. The NSG showed maximum increase in hardness up to 7.9% while MLG showed up to 18.3%. It shows that MLG is more effective in increasing the hardness of samples compared with NSG. The relatively lower increase in hardness by NSG can be attributed to corrugated structure of NSG. The MLG is relatively smooth and flat as schematically shown in Fig. 7 (d) and SEM image shown in Fig. 1 (c). The indenter sits perfectly on MLG sheets and MLG can offer sufficient amount of resistance toward indentation owing to its very high strength and modulus values.[57–59] Therefore, MLG showed a significant increase in hardness. On the contrary, NSG is heavily corrugated as schematically shown in Fig. 7 (e) and SEM image shown in Fig. 1 (f). In this case, the indenter faces a little resistance due to the sponge-like structure. Similar results were reported by Jana and Zhong.[60] They expanded the graphite flakes at 1000 °C for 30 s in an auto-controlled electronic furnace.[60] The cause behind this expansion was $CO_2$ which was generated from the decomposition of intercalant between graphite sheets. The augmentation of $CO_2$ in the interstices caused exfoliation of graphene sheets. The expanded graphite flakes were ground down to nm scale using a planetary ball mill and the product was called as "puffed" graphite.[60] The elastic modulus and hardness of puffed graphite as calculated by nanoindentation test were found to be lower than that of precursor graphite flakes.[60] It is also possible that indenter may go inside the trenches and does not come in contact

with NSG at all. However, it should follow with no increase in hardness. The hardness reported here is the average of 20 values. Therefore, it indicates that filler is dispersed to an extent that indenter gets in contact with the filler and significantly affects hardness. A relatively lower increase caused by NSG than MLG indicates that indenter did not face much resistance in case of NSG because of its spongy structure. As the polymer has lower hardness, therefore the overall increase in hardness observed in case of NSG is lower than that observed with MLG. As MLG and NSG had different morphology and particle size distribution, the fracture patterns observed in tensile specimens were also different. The two mainly observed fracture modes are schematically shown in Fig. 7 (f-i). When a structural member is subjected to axial loading as shown in Fig. 7 (f), fracture takes place when the loading exceeds UTS. When the material is brittle, the crack proceeds in straight path as shown in Fig. 7 (g). On the other hand, when material is soft, crack tip is followed by a plastic work zone.[61] Because of this plasticity, a rough and corrugated surface results as shown in Fig. 7 (h) whose top view is shown in Fig. 7 (i). The crack is intergranular and dimple fracture occurs which is an indication of ductile fracture.

## Conclusions

The damage tolerance and fracture toughness of epoxy nanocomposites are strongly dependent on morphological features of carbonaceous materials. A significant increase in mechanical properties with NSG indicates that an efficient network of reinforcement particles can be achieved by using wide particle size distribution. When particle size distribution is narrow, the voids between the particles would not be filled and those filler-free or empty locations will be a preferred route for the cracks to surmount the reinforcement particles. On the other hand, when reinforcement has wide size distribution, the finer particles can occupy the empty spaces in between large particles. It increases the filling ratio and makes an efficiently connected network of reinforcement. The wider morphology of reinforcement increases packing density, interfacial area, and mechanical interlocking with the polymer chains. In addition, morphologically modified particles can significantly increase the coefficient of friction between reinforcement-reinforcement and reinforcement-matrix interfaces. A large amount of energy will be dissipated to work against friction that will increase the toughness of the samples prior to fracture. The NSG showed maximum increase in hardness up to 7.9% while MLG showed up to 18.3%. It shows that MLG is more effective in increasing the hardness of samples compared with NSG. The MLG and NSG increased the storage modulus and $T_g$ while loss modulus and Tanδ decreased. SEM images of fractured surfaces of tensile specimens showed that fracture mode was significantly altered by MLG and NSG. Monolithic epoxy showed river markings that indicate typical brittle fracture observed in epoxy. With the incorporation of MLG, no specific orientation of crack propagation was observed. With the addition of NSG, a very rough dimple-like fracture surface was observed which shows that fracture mode shifted from brittle to ductile fracture.

## Acknowledgements

The authors would like to thank the Department of Mechanical and Construction Engineering, Northumbria University, UK for the provision of research facilities, without which the analysis of relevant data was not possible.

## References

1 E. Cerda and L. Mahadevan, *Phys. Rev. Lett.*, 2003, **90**, 074302.
2 A. S. Balankin and S. H. Orlando, *Phys. Rev. E*, 2008, **051124**, 77.
3 Z. Qin and M. Buehler, *Mol. Simul.*, 2012, **38**, 695–703.
4 R. Jabari Seresht, M. Jahanshahi, A. Rashidi and A. A. Ghoreyshi, *Appl. Surf. Sci.*, 2013, **276**, 672–681.
5 M. U. M. Patel, N. D. Luong, J. Seppälä, E. Tchernychova and R. Dominko, *J. Power Sources*, 2014, **254**, 55–61.
6 K. Zhang, X. Duan, X. Zhu, D. Hu, J. Xu, L. Lu, H. Sun and L. Dong, *Synth. Met.*, 2014, **195**, 36–43.
7 S. W. Cranford and M. J. Buehler, *Phys. Rev. B - Condens. Matter Mater. Phys.*, 2011, **84**.
8 K. T. Faber and A. G. Evans, *Acta Metall.*, 1983, **31**, 565–576.
9 K. T. Faber and A. G. Evans, *Acta Metall.*, 1983, **31**, 577–584.
10 M. J. Palmeri, K. W. Putz and L. C. Brinson, *ACS Nano*, 2010, **4**, 4256–64.
11 S. Cranford and M. J. Buehler, *Model. Simul. Mater. Sci. Eng.*, 2011, **19**, 054003.
12 D. Lee, X. Zou, X. Zhu, J. W. Seo, J. M. Cole, F. Bondino, E. Magnano, S. K. Nair and H. Su, *Appl. Phys. Lett.*, 2012, **101**, 021604.
13 M. Becton, L. Zhang and X. Wang, *Chem. Phys. Lett.*, 2013, **584**, 135–141.
14 J. Zhao, B. Yang, Z. Zheng, J. Yang, Z. Yang, P. Zhang, W. Ren and X. Yan, *ACS Appl. Mater. Interfaces*, 2014, **6**, 9890–9896.
15 W. Bao, F. Miao, Z. Chen, H. Zhang, W. Jang, C. Dames and L. C. Ning, *Nat. Nanotechnol.*, 2009, **4**, 562 – 566.
16 S. Cranford, D. Sen and M. J. Buehler, *Appl. Phys. Lett.*, 2009, **95**, 2013–2016.
17 J. C. Meyer, A. k. Geim, M. I. Katsnelson, K. S. Novoselov, T. J. Booth and S. Roth, *Nature*, 2007, **446**, 60–63.
18 M. Becton, L. Zhang and X. Wang, *Phys. Chem. Chem. Phys.*, 2015, **17**, 6297–6304.
19 E. Perim, L. D. Machado and D. S. Galvao, 2015, 1–17.
20 S. Chandrasekaran, N. Sato, F. Tölle, R. Mülhaupt, B. Fiedler and K. Schulte, *Compos. Sci. Technol.*, 2014, **97**, 90–99.
21 *ASM Handbook Vol. 21, Composites*, 2001.
22 A. V. Naumov, S. Ghosh, D. a. Tsyboulski, S. M. Bachilo and R. B. Weisman, *ACS Nano*, 2011, **5**, 1639–1648.
23 Z. A. Ghaleb, M. Mariatti and Z. M. Ariff, *Compos. Part A Appl. Sci. Manuf.*, 2014, **58**, 77–83.
24 J. a. King, D. R. Klimek, I. Miskioglu and G. M. Odegard, *J. Appl. Polym. Sci.*, 2013, **128**, 4217–4223.
25 X. Wang, L. Song, W. Pornwannchai, Y. Hu and B. Kandola, *Compos. Part A Appl. Sci. Manuf.*, 2013, **53**, 88–96.
26 W. P. Serena Saw and M. Mariatti, *J. Mater. Sci. Mater. Electron.*, 2011, **23**, 817–824.
27 I. Zaman, H.-C. Kuan, Q. Meng, A. Michelmore, N. Kawashima, T. Pitt, L. Zhang, S. Gouda, L. Luong and J. Ma, *Adv. Funct. Mater.*,

2012, **22**, 2735–2743.
28 M. R. Loos, L. A. F. Coelho, S. H. Pezzin and S. C. Amico, *Polímeros*, 2008, **18**, 76–80.
29 K. Lau, M. Lu, H. Cheung, F. Sheng and H. Li, *Compos. Sci. Technol.*, 2005, **65**, 719–725.
30 S. Hong and C. Wu, *Thermochim. Acta*, 1998, **316**, 167–175.
31 A. Ciesielski and P. Samorì, *Chem. Soc. Rev.*, 2014, **43**, 381–98.
32 Y. Hernandez, V. Nicolosi, M. Lotya, F. M. Blighe, Z. Sun, S. De, I. T. McGovern, B. Holland, M. Byrne, Y. K. Gun'Ko, J. J. Boland, P. Niraj, G. Duesberg, S. Krishnamurthy, R. Goodhue, J. Hutchison, V. Scardaci, A. C. Ferrari and J. N. Coleman, *Nat. Nanotechnol.*, 2008, **3**, 563–568.
33 D. a C. Brownson, D. K. Kampouris and C. E. Banks, *J. Power Sources*, 2011, 196, 4873–4885.
34 L. Peponi, D. Puglia, L. Torre, L. Valentini and J. M. Kenny, *Mater. Sci. Eng. R Reports*, 2014, **85**, 1–46.
35 K. Chrissafis and D. Bikiaris, *Thermochim. Acta*, 2011, **523**, 1–24.
36 B. Yu, X. Wang, X. Qian, W. Xing, H. Yang, L. Ma, Y. Lin, S. Jiang, L. Song, Y. Hu and S. Lo, *RSC Adv.*, 2014, **4**, 31782.
37 X. F. Yao, D. Zhou and H. Y. Yeh, *Aerosp. Sci. Technol.*, 2008, **12**, 223–230.
38 B. C. Kim, S. W. Park and D. G. Lee, *Compos. Struct.*, 2008, **86**, 69–77.
39 F. H. Gojny, M. H. G. Wichmann, U. Köpke, B. Fiedler and K. Schulte, *Compos. Sci. Technol.*, 2004, **64**, 2363–2371.
40 M. J. Mathews and S. R. Swanson, *Compos. Sci. Technol.*, 2007, **67**, 1489–1498.
41 *ASM Handbook, Vol. 5. Surface Engineering*, 1994.
42 J. Karger-Kocsis, H. Mahmood and A. Pegoretti, *Prog. Mater. Sci.*, 2015, **73**, 1–43.
43 S. I. Moon and J. Jang, *J. Mater. Sci.*, 1999, **34**, 4219–4224.
44 M. Nardin and I. M. Ward, *Mater. Sci. Technol.*, 1987, **3**, 814–826.
45 N. H. Ladizesky and I. M. Ward, *J. Mater. Sci.*, 1989, **24**, 3763–3773.
46 D. W. Woods and I. M. Ward, *Surf. Interface Anal.*, 1993, **20**, 385–392.
47 B. Tissington, G. Pollard and I. M. Ward, *J. Mater. Sci.*, 1991, **26**, 82–92.
48 X. Wang, J. Jin and M. Song, *Carbon N. Y.*, 2013, **65**, 324–333.
49 J. Wei, R. Atif, T. Vo and F. Inam, 2015, **2015**.
50 J. Wei, T. Vo and F. Inam, *RSC Adv.*, 2015, **5**, 73510–73524.
51 Y. Zhang, Y. Wang, J. Yu, L. Chen, J. Zhu and Z. Hu, *Polymer (Guildf).*, 2014, **55**, 4990–5000.
52 L.-C. Tang, Y.-J. Wan, D. Yan, Y.-B. Pei, L. Zhao, Y.-B. Li, L.-B. Wu, J.-X. Jiang and G.-Q. Lai, *Carbon N. Y.*, 2013, **60**, 16–27.
53 H. Feng, X. Wang and D. Wu, *Ind. Eng. Chem. Res.*, 2013, **52**, 10160–10171.
54 *ASM Handbook, Vol. 12. Fractography.*, 2001.
55 H. Y. Sohn and C. Moreland, *Can. J. Chem. Eng.*, 1968, **46**, 162–167.
56 D. J. Cumberland, R. J. Crawford and D. Sprevak, *Eur. Polym. J.*, 1989, **25**, 1173–1182.
57 A. Tabarraei, S. Shadalou and J.-H. Song, *Comput. Mater. Sci.*, 2015, **96**, 10–19.
58 G. Dai and L. Mishnaevsky, *Comput. Mater. Sci.*, 2014, **95**, 684–692.
59 B. Mortazavi and G. Cuniberti, *Nanotechnology*, 2014, **25**, 215704.
60 S. Jana and W.-H. Zhong, *Mater. Sci. Eng. A*, 2009, **525**, 138–146.
61 B. Cotterell, *Eng. Fract. Mech.*, 2002, **69**, 533–553.

## Graphical abstract statement

The mechanical properties of epoxy nanocomposites can be significantly altered by tailoring the morphological features of carbonaceous fillers.